Syntheses, Structure, Magnetism, and Optical Properties of the Ordered Mixed-Lanthanide Sulfides γ-LnLn'S_3 (Ln = La, Ce; Ln' = Er, Tm, Yb)

Geng Bang Jin,[†] Eun Sang Choi,[‡] Robert P. Guertin,[§] James S. Brooks,[‡] Travis H. Bray,[†] Corwin H. Booth,[£] and Thomas E. Albrecht-Schmitt[†,*]

[†]Department of Chemistry and Biochemistry and the E. C. Leach Nuclear Science Center, Auburn University, Auburn, Alabama 36849

[‡]Department of Physics and National High Magnetic Field Laboratory, Florida State University, Tallahassee, Florida 32310

[§]Department of Physics and Astronomy, Tufts University, Medford, Massachusetts 02155

[£]Chemical Sciences Division, Lawrence Berkeley National Laboratory, 1 Cyclotron Rd., Berkeley, CA 94720

A Submission to Chemistry of Materials

Abstract

γ-LnLn'S_3 (Ln = La, Ce; Ln' = Er, Tm, Yb) have been prepared as dark red to black single crystals by the reaction of the respective lanthanides with sulfur in a Sb_2S_3 flux at 1000 °C. This isotypic series of compounds adopts a layered structure that consists of the smaller lanthanides (Er, Tm, and Yb) bound by sulfide in six- and seven-coordinate environments that are connected together by the larger lanthanides (La and Ce) in eight- and nine-coordinate environments. The layers can be broken down into three distinct one-dimensional substructures containing three crystallographically unique Ln' centers. The first of these is constructed from one-dimensional chains of edge-sharing [Ln'S_7] monocapped trigonal prisms that are joined to equivalent chains via edge-sharing to yield ribbons. There are parallel chains of [Ln'S_6] distorted octahedra that are linked to the first ribbons through corner-sharing. These latter units also share corners with a one-dimensional ribbon composed of parallel chains of [Ln'S_6] polyhedra that edge-share both in the direction of chain propagation and with adjacent identical chains. Magnetic susceptibility measurements show Curie-Weiss behavior from 2 to 300 K with antiferromagnetic coupling, and no evidence for magnetic ordering. The θ_p values range from –0.4 to –37.5 K, and spin-frustration may be indicated for the Yb-containing compounds. All compounds show magnetic moments substantially reduced from those calculated for the free ions. The optical band gaps for γ-LaLn'S_3 (Ln' = Er, Tm, Yb) are approximately 1.6 eV, whereas γ-CeLn'S_3 (Ln' = Er, Tm, Yb) are approximately 1.3 eV.

INTRODUCTION

The structures and electronic properties of lanthanide chalcogenides are exquisitely tunable, allowing for the rational development of new optical[1-14] and magnetic materials.[13,15-23] Even compositional simple binary sesquisulfides of the trivalent lanthanides can have remarkably complex structures, and are found in at least seven different modifications ranging from A-type Ln_2S_3,[24] where the lanthanides are found in seven- and eight-coordinate geometries, to T-type[25] compounds that adopt the corundum structure with six-coordinate lanthanides.[24-30] The structural complexity of the sesquisulfides is aptly illustrated by the F-type compounds that contain Ln^{3+} ions in three different environments as distorted octahedra and mono- and bicapped trigonal prisms.[29,30] These structural features can be exploited for the development of potentially ordered ternary and quaternary mixed-lanthanide phases by systematically substituting smaller ions into lower coordination number sites and larger ions into higher coordination number sites (e.g. $CeYb_3S_6$).[31-33] However, disordering of the Ln^{3+} ions becomes increasingly problematic as the difference in the size of the ions becomes too small. While disorder of these ions can be advantageous from the perspective of doping (e.g. in Ln:YAG),[34-36] the preparation of materials where ordering of the lanthanide ions occurs allows for the exploration of structure-property relationships where different Ln^{3+} ions are structurally distinct.

In addition to disordered ternary mixed-lanthanide sesquisulfides adopting the F-Tm_3S_6 (e.g. $ScEr_3S_6$)[29,33] and $CeTmS_3$[37] structures there are several known families of compounds where there is strong evidence for ordering of different Ln^{3+} ions. This is best known from α- and β-$LnLn'S_3$.[39-43] α-$LnLn'S_3$ (Ln = Y, La, Ce, Nd; Ln' = Sc, Yb) adopts the ordered $GdFeO_3$[38] structure type.[39-41] Changes in bonding in ternary mixed-lanthanide sesquisulfides of a single composition can have dramatic effects on the electronic properties of these solids. For example,

the band gap of β-$LaYbS_3$ is different than that of γ-$LaYbS_3$ (*vide infra*). Furthermore, there is also evidence supporting geometric spin-frustration in interlanthanide compounds.[43] In an effort to explore the possibility of spin-frustration and possible magnetic coupling between different lanthanide ions, we have prepared a series of new ordered mixed-lanthanide chalcogenides. Herein we disclose the syntheses, structure, magnetic susceptibility, and optical properties of the interlanthanide sulfides γ-$LnLn'S_3$ (Ln = La, Ce; Ln' = Er, Tm, Yb), and discuss the relationships between these details and those known for other materials in this class.

EXPERIMENTAL

Materials. La (99.9%, Alfa-Aesar), Ce (99.9%, Alfa-Aesar), Er (99.9%, Alfa-Aesar), Tm (99.9%, Alfa-Aesar), Yb (99.9%, Alfa-Aesar), S (99.5%, Alfa-Aesar), and Sb (99.5%, Alfa-Aesar) were used as received. Sb_2S_3 was prepared from the direct reaction of the elements in sealed fused-silica ampoules at 850 °C.

Syntheses of γ-$LnLn'S_3$ (Ln = La, Ce; Ln' = Er, Tm, Yb). 200 mg of Ln, Ln', S, and Sb_2S_3 in a ratio of 1:1:3:0.5 were loaded into fused-silica ampoules in an argon-filled glovebox. The ampoules were sealed under vacuum and heated in a programmable tube furnace. The following heating profile was used: 2 °C/min to 500 °C (held for 1 h), 0.5 °C/min to 1000 °C (held for 5 d), 0.04 °C/min to 550 °C (held for 2 d), and 0.5 °C/min to 24 °C. In all cases high yields of dark red/black prisms of γ-$LnLn'S_3$ and unreacted Sb_2S_3 were obtained. The desired products can be separated from the flux during the cooling process by slightly tilting the furnace, which allows the flux to flow to the bottom of the tubes leaving crystals of γ-$LnLn'S_3$ behind, minimizing the need for manual separation of solids. Powder X-ray diffraction measurements were used to confirm phase purity by comparing the powder patterns calculated from the single crystal X-ray

structures with the experimental data. Semi-quantitative SEM/EDX analyses were performed using a JEOL 840/Link Isis or JEOL JSM-7000F instrument. Ln, Ln', and S percentages were calibrated against standards. Sb was not detected in the crystals. The Ln:Ln':S ratios were determined to be approximately 1:1:3 from EDX analyses.

Crystallographic Studies. Single crystals of γ-$LnLn'S_3$ (Ln = La, Ce; Ln' = Er, Tm, Yb) were mounted on glass fibers with epoxy and optically aligned on a Bruker APEX single crystal X-ray diffractometer using a digital camera. Initial intensity measurements were performed using graphite monochromated Mo Kα (λ = 0.71073 Å) radiation from a sealed tube and monocapillary collimator. SMART (v 5.624) was used for preliminary determination of the cell constants and data collection control. The intensities of reflections of a sphere were collected by a combination of 3 sets of exposures (frames). Each set had a different ϕ angle for the crystal and each exposure covered a range of 0.3° in ω. A total of 1800 frames were collected with exposure times per frame of 10 or 20 seconds depending on the crystal.

For γ-$LnLn'S_3$ (Ln = La, Ce; Ln' = Er, Tm, Yb), determination of integrated intensities and global refinement were performed with the Bruker SAINT (v 6.02) software package using a narrow-frame integration algorithm. These data were treated first with a face-index numerical absorption correction using XPREP,[44] followed by a semi-empirical absorption correction using SADABS.[45] The program suite SHELXTL (v 6.12) was used for space group determination (XPREP), direct methods structure solution (XS), and least-squares refinement (XL).[44] The final refinements included anisotropic displacement parameters for all atoms and secondary extinction. Some crystallographic details are given in Table 1. As an example, atomic coordinates and equivalent isotropic displacement parameters for γ-$LaYbS_3$ are given in Table 2. It is important to note that we have expressed the formula of these compounds as γ-$LnLn'S_3$,

which implies $Z = 12$. However, a more accurate description would be $Ln_3Ln'_3S_9$ with $Z = 4$, because there are three crystallographically unique sites for each type of lanthanide ion. We use γ-$LnLn'S_3$ here so that comparisons with other 1:1:3 interlanthanide compounds can be made more easily. Additional crystallographic details can be found in the Supporting Information.

Powder X-ray Diffraction. Powder X-ray diffraction patterns were collected with a Rigaku Miniflex powder X-ray diffractometer using Cu Kα (λ = 1.54056 Å) radiation.

Magnetic Susceptibility Measurements. Magnetism data were measured on powders in gelcap sample holders with a Quantum Design MPMS 7T magnetometer/susceptometer between 2 and 300 K and in applied fields up to 7 T. DC temperature dependent susceptibility measurements were made under zero-field-cooled conditions with an applied field of 0.1 T. Susceptibility values were corrected for the sample diamagnetic contribution according to Pascal's constants[46] as well as for the sample holder diamagnetism. θ_p values were obtained from extrapolations from fits between 100 to 300 K.

UV-vis-NIR Diffuse Reflectance Spectroscopy. The diffuse reflectance spectra for γ-$LnLn'S_3$ (Ln = La, Ce; Ln' = Er, Tm, Yb) were measured from 200 to 1500 nm using a Shimadzu UV3100 spectrophotometer equipped with an integrating sphere attachment. The Kubelka-Monk function was used to convert diffuse reflectance data to absorption spectra.[47]

RESULTS AND DISCUSSION

Effects of Synthetic Parameters on Product Composition and Structure. γ-$LnLn'S_3$ (Ln = La, Ce; Ln' = Er, Tm, Yb) were synthesized via the reaction of the respective lanthanides with elemental sulfur in a Sb_2S_3 flux at 1000 °C. Conveniently, when the reactions are maintained at a slight angle, on cooling, the majority of the flux moves to the bottom of the

ampoules leaving isolated crystals of γ-LnLn'S_3 (Ln = La, Ce; Ln' = Er, Tm, Yb). In sharp contrast, in the absence of the flux, microcrystalline mixed-lanthanide sulfides phases form, but the yield is very low, and the crystals are far too small to investigate using single crystal X-ray diffraction. Furthermore, because there are several recognized phases for mixed-lanthanide sulfides with compositions close to 1:1:3,[37,41-43] the products of these direct reactions are also ambiguous. The choice of flux has proven to be critical in this system as demonstrated by the replacement of Sb_2S_3 with CsCl, which instead results in Cs^+ incorporation, and the formation of the quaternary phases $Cs_{0.14-0.17}Ln_{0.26-0.33}YbS_2$ (Ln = La – Yb).[48] A KI flux has been used in the preparation of β-LnYbQ_3 (Ln = La – Sm; Q = S, Se).[43] However, in contrast to the selenides, the yield of β-LaYbS_3 was very low, inhibiting detailed measurements of its electronic properties.[43] It has been previously noted even in binary sesquisulfides that preparative conditions play a dramatic role in the structure type adopted.[27-29] For example, four different forms of Er_2S_3 can be synthesized by varying temperature, pressure, and crystal growth methods.[30]

Product composition and structure were investigated as a function of the size of Ln, Ln', and by the substitution of Se for S. When the size of Ln is decreased slightly (on the order of 0.02 Å) on going from Ce to Pr, ternary phases with the $CeYb_3S_6$ (F-Tm_2S_3) structure-type[29] were found to form. It is important to note that the trivalent ions in this phase are highly disordered.[31,33] For the La-containing phases, when Ln' is increased in size by transitioning from Er to Ho, mixtures of $LaHo_3S_6$ with the $CeYb_3S_6$ structure and γ-LaHo'S_3 crystallize. In contrast, for the Ce-containing phases, when the same substitution of Ho for Er is performed the new phase, δ-CeHoS_3 (CeTmS_3-type[37]), is found. The structure and properties of δ-CeHoS_3 are quite distinct from that of γ-LnLn'S_3 (Ln = La, Ce; Ln' = Er, Tm, Yb), and will be the subject of a subsequent report. In general, when Ln and Ln' become too close in size, we have found that for

those reactions that occur in Sb_2S_3 fluxes, that the yield of the desired ternary phases becomes very low and crystals often do not form.

The substitution of Se for S results in a highly complex $Ln_xLn'_ySe_z$ system. For the La/Yb/Se reaction in a Sb_2Se_3 flux, $La_5Yb_{5-x}Se_7$ with the Y_5S_7 structure-type forms.[49,50] The lanthanide ions in this phase are highly disordered. In the (Ce – Nd)/Yb/Se series the β-$LnYbS_3$ phases are found instead.[43] When the size of Ln' is increased on substituting Tm for Yb the $Ln_{1+x}Tm_{3-x}Se_6$ (Ln = La – Sm) compounds form, which adopt the disordered $CeYb_3S_6$ structure.[31] When the size of Ln' is increased again by replacing Tm with Er, in the La/Er/Se system, $LaErSe_3$ with the δ-$CeHoS_3$ structure crystallizes. As in the sulfide reactions, if the difference in the size of the two lanthanide ions becomes too small, as is the case in Nd/Er/Se, the disordered $CeYb_3S_6$ structure is adopted again (e.g. in $Nd_{1+x}Er_{3-x}Se_6$).

As can be gleaned from the above discussion, there can be sharp demarcations between neighboring lanthanide ions in ternary mixed-lanthanide sulfides and selenides. Notably we have yet to mention the Lu-containing phases in the above discussion. This is because our observations are that these reactions do not follow previously observed trends for mixed-lanthanide phases where there is substantial size mismatch. Instead, we have isolated (in low yield) $LaLu_3S_6$ with the $CeYb_3S_6$ structure, which would normally result from having lanthanides of more similar size, as well as δ-$LnLuS_3$ (Ln = Ce, Pr, Nd). To reiterate, both of these structure-types have lanthanide site positional disorder that is unexpected in this system because these trivalent ions differ by approximately 0.17 Å.

Structural Features of γ-$LnLn'S_3$ (Ln = La, Ce; Ln' = Er, Tm, Yb). The isotypic series, γ-$LnLn'S_3$ (Ln = La, Ce; Ln' = Er, Tm, Yb), crystallize in the centrosymmetric orthorhombic space group *Pnma*. While this structure is a dense layered network, we will

describe it in terms of lower-dimensional substructures so that the subtleties of bonding in these complex materials can be better understood. It is important to note from the outset that the structure of γ-$LnLn'S_3$ is dramatically different from that of both α- and β-$LnLn'S_3$.[41-43] γ-$LnLn'S_3$ adopts the same space group as α-$LnLn'S_3$. However, there is only one distinct crystallographic site for each of the Ln and Ln' centers (two total sites). The same is also true for the layered structure of β-$LnLn'S_3$ ($UFeS_3$-type[51]).[43] In contrast, γ-$LnLn'S_3$ can also be expressed as $Ln_3Ln'_3S_9$ because there are three crystallographically unique sites for both the Ln and Ln' atoms. Ordering of two different Ln^{3+} ions in a lattice is often difficult to achieve owing to the similarities in the structural chemistry of the trivalent lanthanide ions (*vide supra*). In α-, β-, and γ-$LnLn'S_3$, ordering of the Ln and Ln' sites is accomplished by choosing lanthanide ions at opposite ends of the series. Typically earlier, larger lanthanides favor higher coordination numbers than the later, smaller ions. In α-$LnLn'S_3$ the two different lanthanide ions are actually both six-coordinate, however the larger ions are found in trigonal prisms, whereas the small ones are found in octahedral environments. In contrast, the larger trivalent lanthanides in β-$LnLn'S_3$ have eight close neighbors, and the Yb^{3+} ions only have six. γ-$LnLn'S_3$ follows the same general trends as β-$LnLn'S_3$ by placing the larger ions in eight- and nine-coordinate environments, and the smaller ions are seven- and six-coordinate geometries.

We choose here to adopt the same convention as used for β-$LnLn'S_3$ to describe the structure of γ-$LnLn'S_3$, which is as two-dimensional $^{2}_{\infty}[Ln'_3S_9]^{9-}$ (Ln' = Er, Tm, Yb) layers that extend in the [*bc*] plane that contain the smaller lanthanide ions that are separated by larger Ln^{3+} ions, La^{3+} and Ce^{3+}, as is depicted in Figure 1c. For comparison, α- and β-$LnLn'S_3$ are shown in Figures 1a and 1b. There are no S–S bonds in α-, β-, or γ-$LnLn'S_3$, and therefore the oxidation

states in these compounds can be assigned as +3/+3/-2. This designation is confirmed by both bond-valence sum calculations[52,53] and by magnetic susceptibility measurements (*vide infra*).

An individual $^{2}_{\infty}[Ln'_3S_9]^{9-}$ (Ln' = Er, Tm, Yb) layer viewed down the *a* axis is shown in Figure 2. As can be seen in this sketch, this layer is constructed from edge-sharing double chains of [Ln'S_7] monocapped trigonal prisms (A) and double chains of [Ln'S_6] octahedra (B) that are linked by single chains of [Ln'S_6] octahedra (C) in the manner of ACBCA. The central C chains share corners with the A and B chains. The $^{2}_{\infty}[Ln'_3S_9]^{9-}$ layers in γ-LnLn'S_3 are more buckled than those in β-LnLn'S_3, because the chains of [Ln'S_6] octahedra (C) share both axial and equatorial corners with the double chains (A and B). In β-LnLn'S_3 only axial (trans) atoms are corner-sharing. For reference, in γ-LaYbS_3 the Yb–S bond distance for Yb(1), Yb(2), and Yb(3) range from 2.5979(19) to 2.783(2) Å, and are normal.

As shown in Figure 3, the larger lanthanides La^{3+} and Ce^{3+} (Ln(1), Ln(2), and Ln(3)) ions are found in coordination environments with more neighbors than the Er^{3+}, Tm^{3+}, and Yb^{3+} ions. There is some difficulty in precisely describing the coordination number of the Ln(1) centers. These Ln^{3+} cations are located within highly distorted tricapped trigonal prismatic environments. Two of the Ln···S capping contacts, however, are substantially longer than those that define the trigonal prism. For example, in γ-LaYbS_3 the short La–S bonds range from 2.892(2) to 3.062(3) Å, whereas the longer contacts are 3.552(3) and 3.813(3) Å. The longest contact should probably not be considered as important. The Ln(2) and Ln(3) atoms, however, are clearly eight-coordinate, and occur as bicapped trigonal prisms with La–S bonds ranging from 2.856(3) to 3.037(2) Å for La(2), and from 2.844(2) to 3.124(3) Å for La(3) in γ-LaYbS_3. The transitions between α-LnLn'S_3, β-LnLn'S_3, and γ-LnLn'S_3 represent systematic increases in the average coordination numbers of the lanthanides, leading to more efficient packing and increased

densities in this single compositional family. For the sake of brevity, we do not provide a list of selected bond distances for all six compounds, but these are available in the Supporting Information.

Magnetic Properties of γ-LnLn'S_3 (Ln = La, Ce; Ln' = Er, Tm, Yb). At first glance the magnetic behavior of γ-LnLn'S_3 (Ln = La, Ce; Ln' = Er, Tm, Yb) seem relatively uninteresting as there is no indication of long-range magnetic ordering down to 2 K, as shown in Figure 4. However, the θ_p parameters are atypical for some of these compounds. The θ_p values are –0.4, –6.7, –32.1, –18.7, –14.6, –37.5 K, for γ-$LaErS_3$, γ-$LaTmS_3$, γ-$LaYbS_3$, γ-$CeErS_3$, γ-$CeTmS_3$, and γ-$CeYbS_3$, respectively. The θ_p parameters for γ-$LaYbS_3$ and γ-$CeYbS_3$ are quite negative, indicating relatively strong antiferromagnetic coupling between Ln^{3+} ions. In the case of γ-$LaYbS_3$, this interaction must be between Yb^{3+} centers. We observed similar phenomena in $Cs_{0.14\text{-}0.17}Ln_{0.26\text{-}0.33}YbS_2$ (Ln = La – Yb).[48] Despite this strong coupling, short- and long-range order are apparently absent. This behavior is consistent with a geometrically spin-frustrated system. It should be noted that β-$CeYbSe_3$ and β-$SmYbSe_3$ have very large θ_p values of –44.6(9) K and –107.6(4) K without any indication of long-range order down to 5 K.[43]

The origin of potential geometric spin-frustration may lie in the layered substructures found in β-LnLn'S_3 and γ-LnLn'S_3. The Sm network for β-$SmYbSe_3$ is shown in Figure 5a. This drawing shows a layer constructed from triangles. The asymmetry of these triangles is capable of preventing ordering in two-dimensions. Figure 5b shows these layers rotated by 90° with the Yb^{3+} ions further connecting the network to create a system that might be frustrated in all three dimensions. In contrast, the source of geometric spin-frustration in γ-LnLn'S_3 is less obvious. In these phases, there are networks of both squares and triangular within the Yb layers as well as the potential for higher-order frustration via the interlayer Ce^{3+} ions as shown in

Figures 5c and d, respectively. We propose that if spin-frustration is occurring in these compounds that it is within the Yb layers, because γ-$LaYbS_3$ and γ-$CeYbS_3$ have large θ_p values that are quite similar in magnitude, and the La^{3+} ions obviously can not contribute to this behavior. The Yb···Yb distances vary considerably between β-$SmYbSe_3$ and γ-$LaYbS_3$, and are different depending on the substructures that they are present in. In β-$LaYbS_3$ and γ-$LaYbS_3$, the shortest Yb···Yb distances of 3.9238(8) and 3.9847(3) Å, respectively, are similar.

In the absence of appropriate trigonal or hexagonal symmetry the triangular networks in β-$LnLn'S_3$ and γ-$LnLn'S_3$ are necessarily asymmetric. As such, one of the requirements of spin-frustration may not be present, and there may be alternative mechanisms for explaining the large negative θ_p values. The first of these is that this might be an affect of crystal-field splitting of the ground-state of the Yb^{3+} ions. A second, and much more complex, mechanism has also been proposed for the frustrated pyrochlore antiferromagnet, $Tb_2Ti_2O_7$.[54] In this compound there is strong evidence supporting extra perturbative exchange coupling beyond nearest neighbors as well as dipolar interactions that may be the cause of the lack of long-range ordering of the moments.[55]

The calculated free-ion moments for γ-$LaErS_3$, γ-$LaTmS_3$, γ-$LaYbS_3$, γ-$CeErS_3$, γ-$CeTmS_3$, and γ-$CeYbS_3$ are 9.59, 7.57, 4.54, 9.92, 7.98, and 5.20 μ_B, respectively.[56] Not surprisingly the observed moments (8.35, 6.65, 3.98, 9.87, 7.28, and 4.50 μ_B) are notably smaller than the ideal values, most likely because of splitting of the ground state terms for these ions. It would require substantially larger fields than 7 T to obtain full moment values for these compounds. The above calculated values are only true if Ce is trivalent. The single 4f electron in Ce is tenuous at best, and tetravalent Ce carries no moment, in which case the Ce-base compounds would have the same effective moment as the La-based compounds. The isothermal

magnetization measurements also show that the saturation moment is considerably less than the free ion value. Isothermal magnetization measurements carried out to 7 T at 2 K support the conclusions of the effective moment measurements, i.e., that the moments are low.

Optical Properties of γ-LnLn'S_3 (Ln = La, Ce; Ln' = Er, Tm, Yb). The optical band gaps of ternary and quaternary chalcogenides have been shown to be tunable based on the choice of lanthanide ion and chalcogen (e.g. $CsLnZnSe_3$ (Ln = Sm, Tb, Dy, Ho, Er, Tm, Yb, and Y)).[9,11,13,14,57] Based on electronic structure calculations, $CsLnZnSe_3$ are thought to be direct band gap semiconductors.[9] The band gaps for binary lanthanide sesquisulfides are generally indirect.[58] Therefore, both direct and indirect band gap semiconductors are recognized in lanthanide chalcogenides, and they are highly dependent on the structure adopted by the phase.[13,14,55,58] The optical band gaps for γ-LnLn'S_3 (Ln = La, Ce; Ln' = Er, Tm, Yb) were measured using UV-vis-NIR spectroscopy. Unfortunately, the band gaps of α- and β-LnLn'S_3 materials have not been reported; although, β-$LaYbS_3$ is reported to be yellow.[43] Qualitatively, the γ-LaLn'S_3 (Ln' = Er, Tm, Yb) compounds are dark red, whereas the γ-CeLn'S_3 (Ln' = Er, Tm, Yb) compounds are black. Congruent with these visual observations, the measured band gaps for γ-LaLn'S_3 (Ln' = Er, Tm, Yb) are all approximately 1.6 eV. The replacement of La by Ce results in a smaller gap for γ-CeLn'S_3 (Ln' = Er, Tm, Yb) of ~1.3 eV. The apparent fine-structure in these spectra are actually f-f transitions for the lanthanide ions. The band gaps observed for γ-LnLn'S_3 are comparable to the indirect band gaps reported for Nd^{3+}:doped α-Gd_2S_3 (A-type), β-La_2S_3, and γ-Y_2S_3 (D-type).[58] The Ce compounds often show the smallest band gaps of the series owing the high energy of $4f^1$ electron.[59,60] The structural modification that occurs for γ-LnLn'S_3 clearly alters the band gap substantially from that observed for the binary phases.

CONCLUSIONS

The role of reaction conditions (pressure, temperature, flux, etc.) in determining composition and structure in both binary and ternary interlanthanide sesquichalcogenides cannot be over emphasized. We focus here on the use of the new flux, Sb_2S_3, which has been used to prepare γ-$LnLn'S_3$ (Ln = La, Ce; Ln' = Er, Tm, Yb) in high yield. In contrast, when KI is employed as a flux, β-$LaYbS_3$ can only be prepared in low yield, and this medium is more amenable for the syntheses of selenide compounds. Some fluxes, such as CsCl, are in fact reactive, resulting in Cs^+ incorporation into the lanthanide chalcogenide phases, and the formation of quaternary compounds that are illustrated by $Cs_{0.14-0.17}Ln_{0.26-0.33}YbS_2$ (Ln = La – Yb).[48] The use of fluxes provides access to mixed-lanthanide compounds with novel structure types, and is a means of understanding structure-property relationships in these intricate materials.

The structure of γ-$LnLn'S_3$ diverges substantially from previously reported interlanthanide sesquisulfides in that there are three crystallographically unique Ln sites in the structure, whereas α- and β-$LnLn'S_3$ have one site for each type of lanthanide ion.[41-43] Ordering of the Ln^{3+} ions is achieved by placing the larger ions in eight- and nine-coordinate environments, and the smaller ions are seven- and six-coordinate geometries. Table 3 provides a listing of mixed-lanthanide sesquichalcogenides that form under the conditions described in this work, indicating whether ordering of the Ln^{3+} ions is achieved, and the coordination environments of the Ln^{3+} ions. These data apply to solids that form from a Sb_2Q_3 (Q = S, Se) flux at 1000 ºC.

Currently, the most promising application of the mixed-lanthanide chalcogenides is the ability to change, and perhaps systematically vary, the band gap of these semiconductors. This

can be accomplished by both changing the lanthanide, as we demonstrated in this report, and by changing the chalcogenide, whereby the band gap should decrease when heavier chalcogenides are substituted into the structure.[57] Doing this allows materials to be prepared that range from nearly colorless to black. This property is not unique to the present system, but rather applies to many lanthanide compounds. We suggest that the possibility exists for finding interesting electronic phenomena by preparing ordered quaternary interlanthanide sesquichalcogenides with three different lanthanides, which might be accomplished by exploiting structures with three different coordination environments for the Ln^{3+} ions.

Acknowledgment. This work was supported by the U.S. Department of Energy under Grant DE-FG02-02ER45963 through the EPSCoR Program. Funds for purchasing the UV-vis-NIR spectrometer used in these studies were provided through the Chemical Sciences, Geosciences and Biosciences Division, Office of Basic Energy Sciences, Office of Science, Heavy Elements Program, U.S. Department of Energy under Grant DE-FG02-01ER15187. Support was also provided by the Director, Office of Science, Office of Basic Energy Sciences, Chemical Sciences, Geosciences and Biosciences Division, U. S. Department of Energy under Contract No. AC03-76SF00098. JSB and ESC acknowledge support from NSF-DMR 0203532. A portion of this work was performed at the National High Magnetic Field Laboratory, which is supported by the National Science Foundation Cooperative Agreement No. DMR-0084173, by the State of Florida, and by the Department of Energy. RPG acknowledges support from NHMFL Visiting Scientist Award #43.

Supporting Information Available: X-ray crystallographic files in CIF format for γ-LnLn'S_3 (Ln = La, Ce; Ln' = Er, Tm, Yb). This material is available free of charge via the Internet at http://pubs.acs.org. Selected bond distances for γ-LnLn'S_3 (Ln = La, Ce; Ln' = Er, Tm, Yb) are also available in a summary table (S1). Magnetization data for γ-LnLn'S_3 (Ln = La, Ce; Ln' = Er, Tm, Yb) are also provided.

References

1) Isaacs, T. J.; Hopkins, R. H.; Kramer, W. E. *J. Electron. Mater.* **1975**, *4*, 1181.

2) Hautala, J.; Taylor, P. C. *J. Non-Cryst. Solids* **1992**, *141*, 24.

3) Nadler, M. P.; Lowe-Ma, C. K.; Vanderah, T. A. *Mater. Res. Bull.* **1993**, *28*, 1345.

4) Kumta P. N.; Risbud, S. H. *J. Mater. Sci.* **1994**, *29*, 1135.

5) Lowe-Ma, C. K.; Vanderah, T. A.; Smith, T. E. *J. Solid State Chem.* **1995**, *117*, 363.

6) Ueda, K.; Inoue, S.; Hosono, H.; Sarukura, N.; Hirano, H. *Appl. Phys. Lett.* **2001**, *78*, 2333.

7) Inoue, S.; Ueda, K.; Hosono, H.; Hamada, N. *Phys. Rev. B* **2001**, *64*, 245211.

8) Huang, F. Q.; Mitchell, K.; Ibers, J. A. *Inorg. Chem.* **2001**, *40*, 5123.

9) Mitchell, K.; Haynes, C. L.; McFarland, A. D.; Van Duyne, R. P.; Ibers, J. A. *Inorg. Chem.* **2002**, *41*, 1199.

10) Mitchell, K.; Ibers, J. A. *Chem. Rev.* **2002**, *102*, 1929-1952.

11) Mitchell, K.; Huang, F. Q.; McFarland, A. D.; Haynes, C. L.; Somers, R. C.; Van Duyne, R. P.; Ibers, J. A. *Inorg. Chem.* **2003**, *42*, 4109.

12) Ueda, K.; Takafuji, K.; Hiramatsu, H.; Ohta, H.; Kamiya, T.; Hirano, M.; Hosono, H. *Chem. Mater.* **2003**, *15*, 3692.

13) Mitchell, K.; Huang, F. Q.; Caspi, E. N.; McFarland, A. D.; Haynes, C. L.; Somers, R. C.; Jorgensen, J. D.; Van Duyne, R. P.; Ibers, J. A. *Inorg. Chem.* **2004**, *43*, 1082.

14) Yao, J.; Deng, B.; Sherry, L. J.; McFarland, A. D.; Ellis, D. E.; Van Duyne, R. P.; Ibers, J. A. *Inorg. Chem.* **2004**, *43*, 7735.

15) Bronger, W.; Miessen, H.-J.; Schmitz, D. *J. Less-Common Met.* **1983**, *95*, 275.

16) Sutorik, A. C.; Albritton-Thomas, J.; Hogan, T.; Kannewurf, C. R.; Kanatzidis, M. G. *Chem. Mater.* **1996**, *8*, 751.

17) Givord, D.; Courtois, D. *J. Magn. Magn. Mater.* **1999**, *196-197*, 684.

18) Wakeshima, M.; Hinatsu, Y. *J. Solid State Chem.* **2000**, *153*, 330.

19) Tougait, O.; Ibers, J. A. *Inorg. Chem.* **2000**, *39*, 1790.

20) Wakeshima, M.; Hinatsu, Y.; Oikawa, K.; Shimojo, Y.; Morii, Y. *J. Mater. Chem.* **2000**, *10*, 2183.

21) Meng, F.; Hughbanks, T. *Inorg. Chem.* **2001**, *40*, 2482.

22) Wakeshima, M.; Hinatsu, Y.; Ishii, Y.; Shimojo, Y.; Morii, Y. *J. Mater. Chem.* **2002**, *12*, 631.

23) Lau, G. C.; Ueland, B. G.; Freitas, R. S.; Dahlberg, M. L.; Schiffer, P.; Cava, R. J. *Phys. Rev. B* **2006**, *73*, 012413.

24) Sleight, A. W.; Prewitt, C. T. *Inorg. Chem.* **1968**, *7*, 2283.

25) Patrie, M. *Bull. Soc. Chim. Fr.* **1969**, *5*, 1600.

26) Bergman, H. (ed.); *Gmelin Handbook of Inorganic Chemistry, Sc, Y, La-Lu (Rare Earth Elements), System Number 39, C7: Sulfides*, Springer, Berlin/Heidelberg/New York/Tokyo, 1983.

27) Flahaut, J.; Guittard, M.; Patrie, M.; Pardo, M. P.; Golabi, S. M.; Domange, L. *Acta Cryst.* **1965**, *19*, 14.

28) Range, K. J.; Leeb, R. *Z. Naturf. B.* **1975**, *30*, 889.

29) Schleid, T.; Lissner, F. *J. Alloys Compd.* **1992**, *189*, 69.

30) Fang, C. M.; Meetsma, A.; Wiegers, G. A. *J. Alloys Compd.* **1993**, *201*, 255.

31) Rodier, N.; Tien, V. *C. R. Seances Acad. Sci. Ser. C* **1974**, *279*, 817.

32) Rodier, N.; Firor, R. L.; Tien, V.; Guittard, M. *Mat. Res. Bull.* **1976**, *11*, 1209.

33) Rodier, N.; Laruelle, P. *Bull. Soc. fr. de Mineral. Cristallogr.* **1973**, *96*, 30.

34) Hamilton, D. S.; Gayen, S. K.; Pogatshnik, G. J.; Ghen, R. D. *Phys. Rev. B* **1989**, *39*, 8807.

35) Cheung,Y. M.; Gayen, S. K. *Phys. Rev. B* **1994**, *49*, 14827.

36) Schweizer, T.; Mobert, P. E.-A.; Hector, J. R.; Hewak, D. W.; Brocklesby, W. S.; Payne, D. N.; Huber, G. *Phys. Rev. Lett.* **1998**, *80*, 1537.

37) Rodier, N. *Bull. Soc. fr. de Mineral. Cristallogr.* **1973**, *96*, 350.

38) Marezio, M.; Remeika, J. P.; Dernier, P. D. *Acta Crystallogr. B* **1970**, *26*, 2008.

39) Rodier, N.; Laruelle, P. *C. R. Seances Acad. Sci. Ser. C* **1970**, *270*, 2127.

40) Ijdo, D. J. W. *Acta Crystallogr. B* **1980**, *36*, 2403.

41) Rodier, N.; Julien, R.; Tien, V. *Acta Crystallogr. C* **1983**, *39*, 670.

42) Carre, D.; Laruelle, P. *Acta Crystallogr. B* **1974**, *30*, 952.

43) Mitchell, K.; Somers, R.C.; Huang, F. Q.; Ibers, J.A. *J. Solid State Chem.* **2004**,*177*, 709.

44) Sheldrick, G. M. SHELXTL PC, Version 6.12, An Integrated System for Solving, Refining, and Displaying Crystal Structures from Diffraction Data; Siemens Analytical X-Ray Instruments, Inc.: Madison, WI 2001.

45) Sheldrick, G. M. *SADABS* 2001, Program for absorption correction using SMART CCD based on the method of Blessing: Blessing, R. H. *Acta Crystallogr.* **1995**, *A51*, 33.

46) Mulay, L. N.; Boudreaux, E. A. *Theory and Applications of Molecular Diamagnetism*; Wiley–Interscience: New York, 1976.

47) Wendlandt, W. W.; Hecht, H. G.: *Reflectance Spectroscopy*. Interscience Publishers, New York, 1966.

48) Jin, G. B.; Booth, C. H.; Albrecht-Schmitt, T. E. *Phys. Rev. B* manuscript in preparation.

49) Adolphe, C. *C. R. Seances Acad. Sci.* **1961**, *252*, 3266.

50) Rodier, N.; Laruelle, P. *Bull. Soc. Fr. Mineral. Cristallogr.* **1972**, *95*, 548.

51) Noel, H.; Padiou, J. *Acta Crystallogr. B* **1976**, *32*, 1593.

52) Brown, I. D.; Altermatt, D. *Acta Crystallogr*. **1985**, *B41*, 244.

53) Brese, N. E.; O'Keeffe, M. *Acta Crystallogr.* **1991**, *B47*, 192.

54) Gardner, J. S.; Dunsinger, S. R.; Gaulin, B. D.; Gingras, M. J. P.; Greedan, J. E.; Kiefl, R. F.; Lumsden, M. D.; MacFarlane, W. A.; Raju, N. P.; Sonier, J. E.; Swainson, I.; Tun, Z. *Phys. Rev. Lett.* **1999**, *82*, 1012.

55) Gingras, M. J. P.; den Hertog, B. C.; Faucher, M.; Gardner, J. S.; Dunsinger, S. R.; Chang, L. J.; Gaulin, B. D.; Raju, N. P.; Greedan, J. E. *Phys. Rev. B* **2000**, *62*, 6496.

56) Kittel, C. *Introduction to Solid State Physics*, 6th Ed., Wiley, New York, 1986.

57) Deng, B.; Ellis, D.E.; Ibers, J.A. *Inorg. Chem.* **2002**, *41*, 5716.

58) Leiss, M. *J. Phys. C: Solid St. Phys.* **1980**, *13*, 151.

59) Prokofiev, A. V.; Shelykh, A. I.; Golubkov, A. V.; Smirnov, I. A. *J. Alloys Compd.* **1995**, *219*, 172.

60) Prokofiev, A. V.; Shelykh, A. I.; Melekh, B. T. *J. Alloys Compd.* **1996**, *242*, 41.

61) Ito, K.; Tezuka, K.; Hinatsu, Y. *J. Solid State Chem.* **2001**, *157*, 173.

Table 1. Crystallographic Data for γ-LnLn'S_3 (Ln = La, Ce; Ln' = Er, Tm, Yb).

See attached file.

Table 2. Atomic Coordinates and Equivalent Isotropic Displacement Parameters for γ-$LaYbS_3$.

Atom (site)	*x*	*y*	*z*	U_{eq} ($Å^2$)[a]
La(1)	0.15941(4)	0.2500	0.24448(3)	0.00942(16)
La(2)	-0.16994(4)	0.2500	0.41369(3)	0.00593(15)
La(3)	-0.19293(4)	-0.2500	0.08024(3)	0.00787(15)
Yb(1)	0.06664(3)	0.2500	0.42039(2)	0.00756(13)
Yb(2)	-0.09466(3)	-0.2500	0.25016(3)	0.01124(14)
Yb(3)	0.05686(3)	-0.2500	0.06883(2)	0.00886(13)
S(1)	-0.03553(18)	0.2500	0.31730(14)	0.0080(6)
S(2)	0.20923(18)	0.2500	0.48254(14)	0.0083(6)
S(3)	0.04299(18)	0.2500	0.55274(14)	0.0082(6)
S(4)	-0.1778(2)	-0.7500	0.18492(14)	0.0124(6)
S(5)	0.05953(18)	-0.2500	-0.05774(14)	0.0091(6)
S(6)	0.15831(18)	-0.7500	0.06464(15)	0.0104(6)
S(7)	-0.22911(18)	-0.2500	0.32202(14)	0.0076(6)
S(8)	0.14585(18)	-0.2500	0.35127(14)	0.0087(6)
S(9)	0.05085(19)	-0.2500	0.19232(14)	0.0101(6)

[a] U_{eq} is defined as one-third of the trace of the orthogonalized U_{ij} tensor.

Table 3. Comparisons of Ternary Interlanthanide Sesquichalcogenides that Form in a Sb_2Q_3 (Q = S, Se) Flux at 1000 ºC.

Structure type	Compounds	Ordered/Disordered	Coordination
β-$LnLn'S_3$ ($UFeS_3$-type)	$CeYbSe_3$, $PrYbSe_3$, $NdYbSe_3$	Ordered	Ln – 8 Ln′ – 6
γ-$LnLn'S_3$	$LnLn'S_3$ (Ln=La, Ce, Ln′=Er-Yb)	Ordered	Ln – 8, 9 Ln′ – 6, 7
δ-$LnLn'S_3$ ($CeTmS_3$-type)	$La_{5-x}Er_{3+x}Se_{12}$, $Ce_{5-x}Ho_{3+x}Se_{12}$, $Ln_{5-x}Lu_{3+x}S_{12}$ (Ln = Ce, Pr, Nd)	Disordered	Ln – 7, 8 Ln′ – 6, 7
F-Ln_2S_3	$La_{1+x}Lu_{3-x}S_6$, $Pr_{1+x}Tm_{3-x}S_6$ $Ln_{1+x}Yb_{3-x}S_6$ (Ln= Pr-Gd), $Ln_{1+x}Yb_{3-x}Se_6$ (Ln= Sm, Gd) $Ln_{1+x}Tm_{3-x}Se_6$ (Ln= La-Sm), $Nd_{1+x}Er_{3-x}Se_6$	Disordered	Ln – 7, 8 Ln′ – 6, 7
Y_5S_7	$La_5Yb_{5-x}Se_7$	Disordered	Ln – 7 Ln′ – 6, 7

Figure Captions

Figure 1. Views of the structures of a) α-$LnLn'S_3$, b) β-$LnLn'S_3$, and c) γ-$LnLn'S_3$ (Ln = La, Ce; Ln' = Er, Tm, Yb). γ-$LnLn'S_3$ adopts a layered structure with two-dimensional $^{2}_{\infty}[Ln'_3S_9]^{9-}$ (Ln' = Er, Tm, Yb) slabs that extend in the [*bc*] plane that contain the smaller lanthanide ions that are separated by larger Ln^{3+} ions, La^{3+} and Ce^{3+}, as is depicted in Figure 1c.

Figure 2. A depiction of an individual $^{2}_{\infty}[Ln'_3S_9]^{9-}$ (Ln' = Er, Tm, Yb) layer viewed down the *a* axis in γ-$LnLn'S_3$ (Ln = La, Ce; Ln' = Er, Tm, Yb). This layer is constructed from edge-sharing double chains of [$Ln'S_7$] monocapped trigonal prisms (A) and double chains of [$Ln'S_6$] octahedra (B) that are linked by single chains of [$Ln'S_6$] octahedra (C) in the manner of ACBCA. The central C chains share corners with the A and B chains.

Figure 3. Illustrations of the coordination environments for the larger lanthanides, La^{3+} and Ce^{3+}, in γ-$LnLn'S_3$ (Ln = La, Ce; Ln' = Er, Tm, Yb). We use γ-$LaYbS_3$ to represent this family of compounds here.

Figure 4. Temperature dependence of the reciprocal molar magnetic susceptibility for γ-$LnLn'S_3$ (Ln = La, Ce; Ln' = Er, Tm, Yb) under an applied magnetic field of 0.1 T.

Figure 5. a) A view of the layers in Sm-based triangles in β-$SmYbSe_3$. b) A depiction of the interconnection of the Sm layers by Yb^{3+} ions. c) An illustration of the square and triangular

networks in γ-$CeYbS_3$. d) A drawing of the complex three-dimension network in γ-$CeYbS_3$. In all cases the chalcogenide ions have been omitted for clarity.

Figure 6. UV-vis diffuse reflectance spectra of γ-$LnLn'S_3$ (Ln = La, Ce; Ln' = Er, Tm, Yb). (*Denotes detector change.)

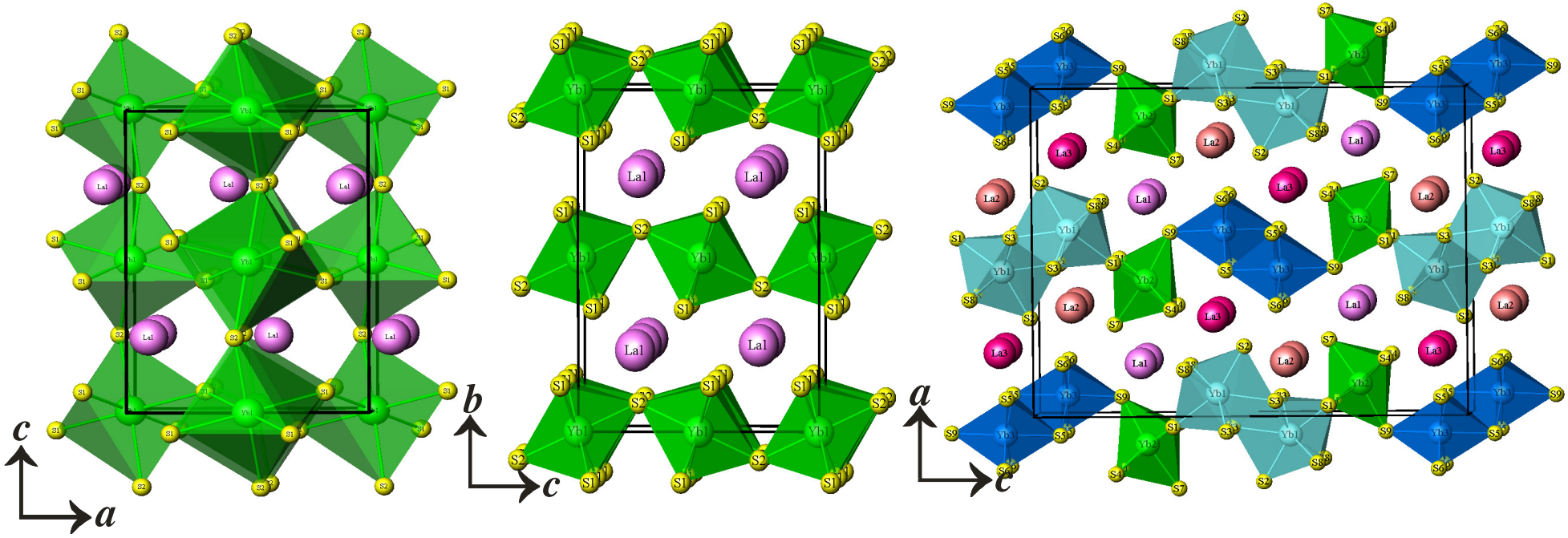

Figure 1.

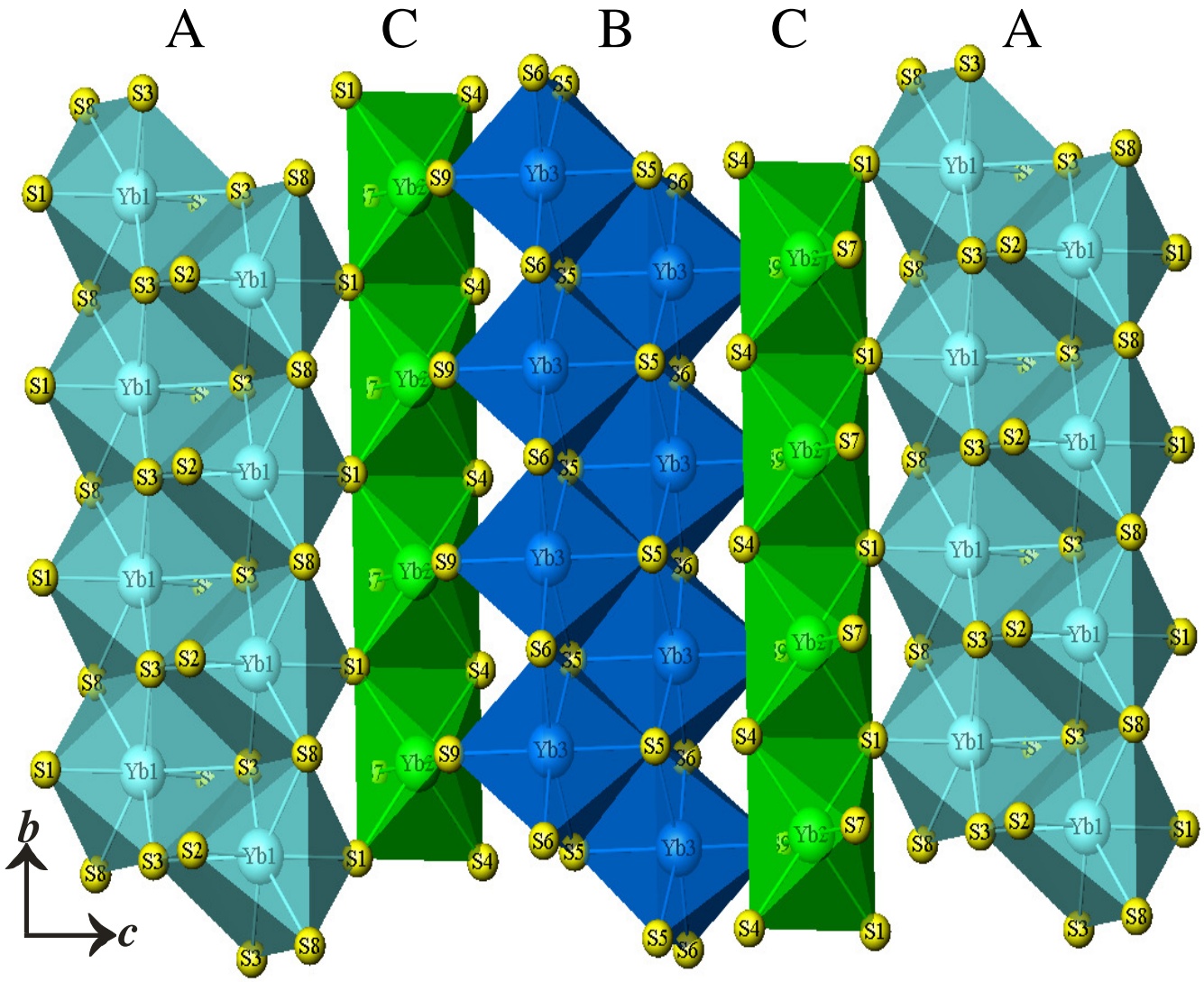

Figure 2.

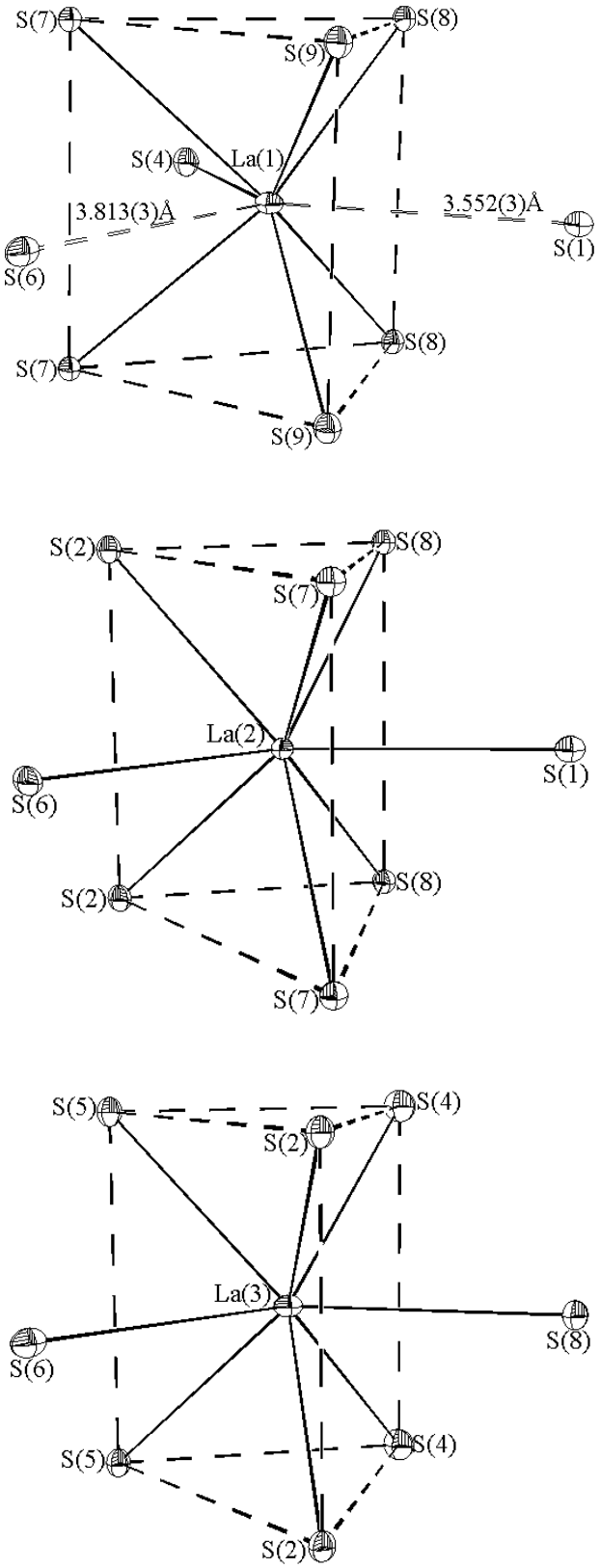
S(7)
S(8)
S(9)
S(4)
La(1)
3.813(3)Å
3.552(3)Å
S(1)
S(6)
S(8)
S(7)
S(9)
S(2)
S(8)
S(7)
La(2)
S(1)
S(6)
S(2)
S(8)
S(7)
S(5)
S(4)
S(2)
La(3)
S(8)
S(6)
S(5)
S(4)
S(2)

Figure 3.

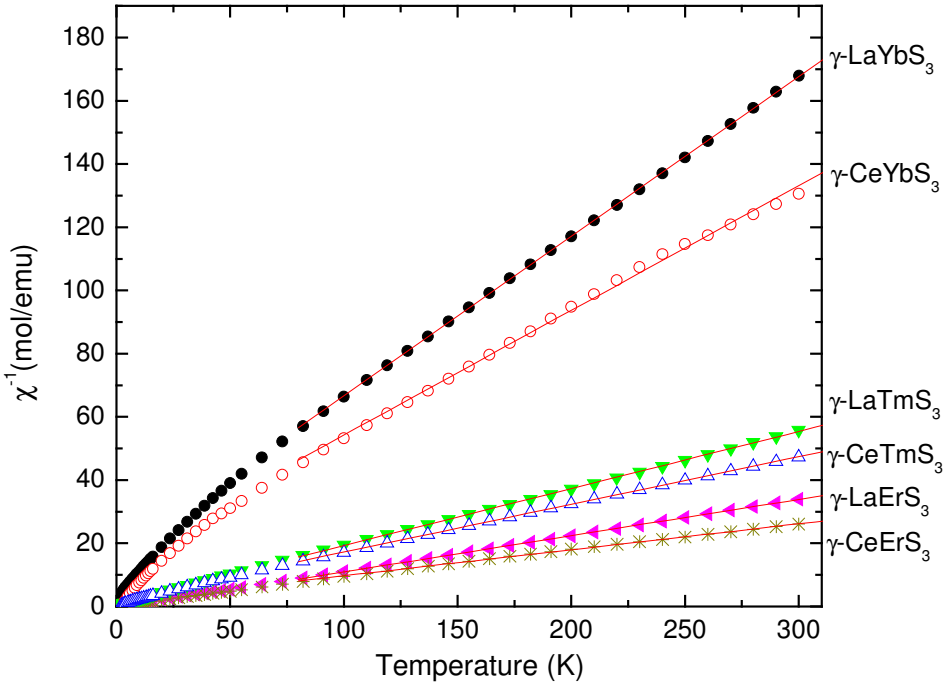
180
160
140
120
100
80
60
40
20
0
0
50
100
150
200
250
300
χ-1(mol/emu)
Temperature (K)
γ-LaYbS3
γ-CeYbS3
γ-LaTmS3
γ-CeTmS3
γ-LaErS3
γ-CeErS3

Figure 4.

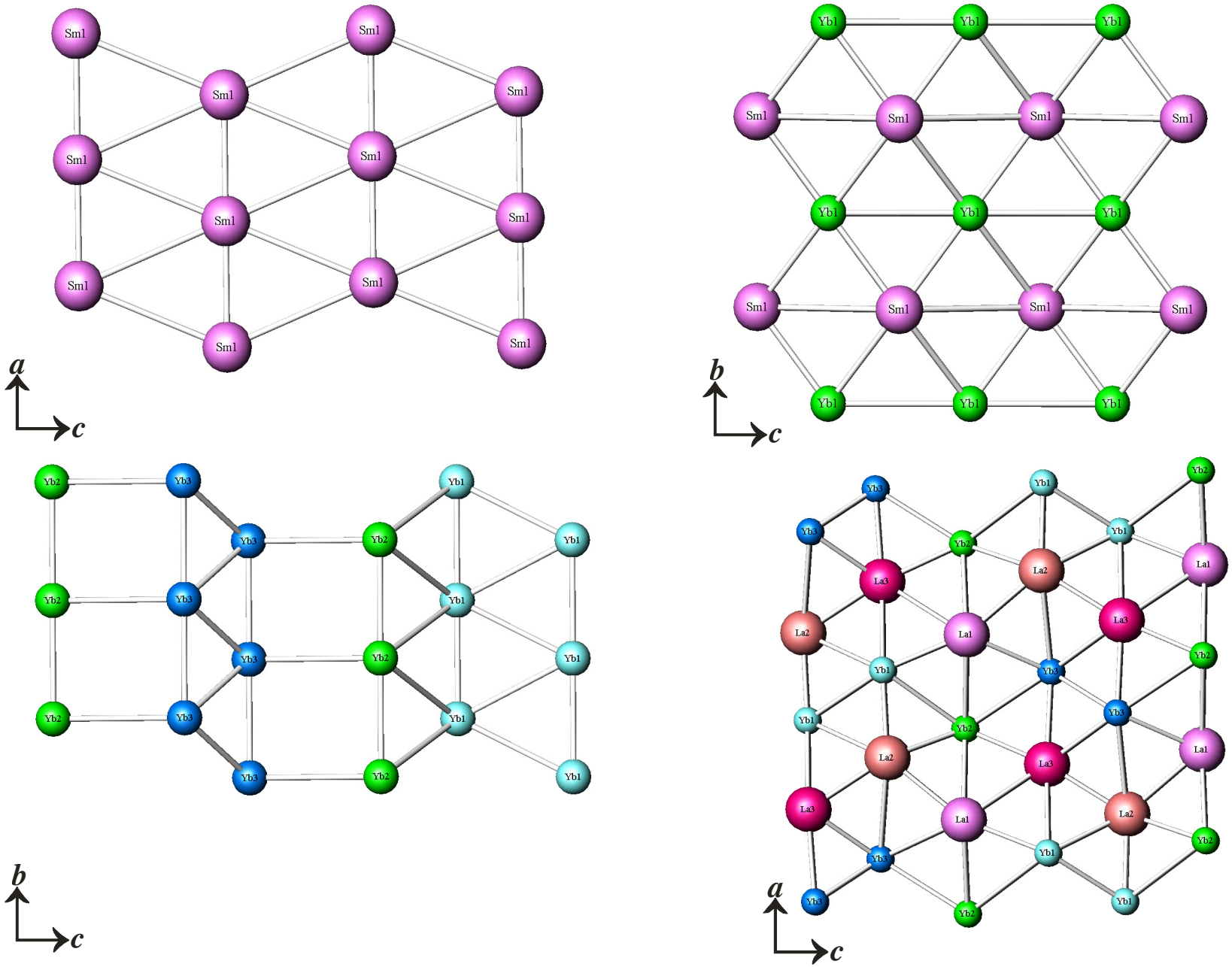

Figure 5.

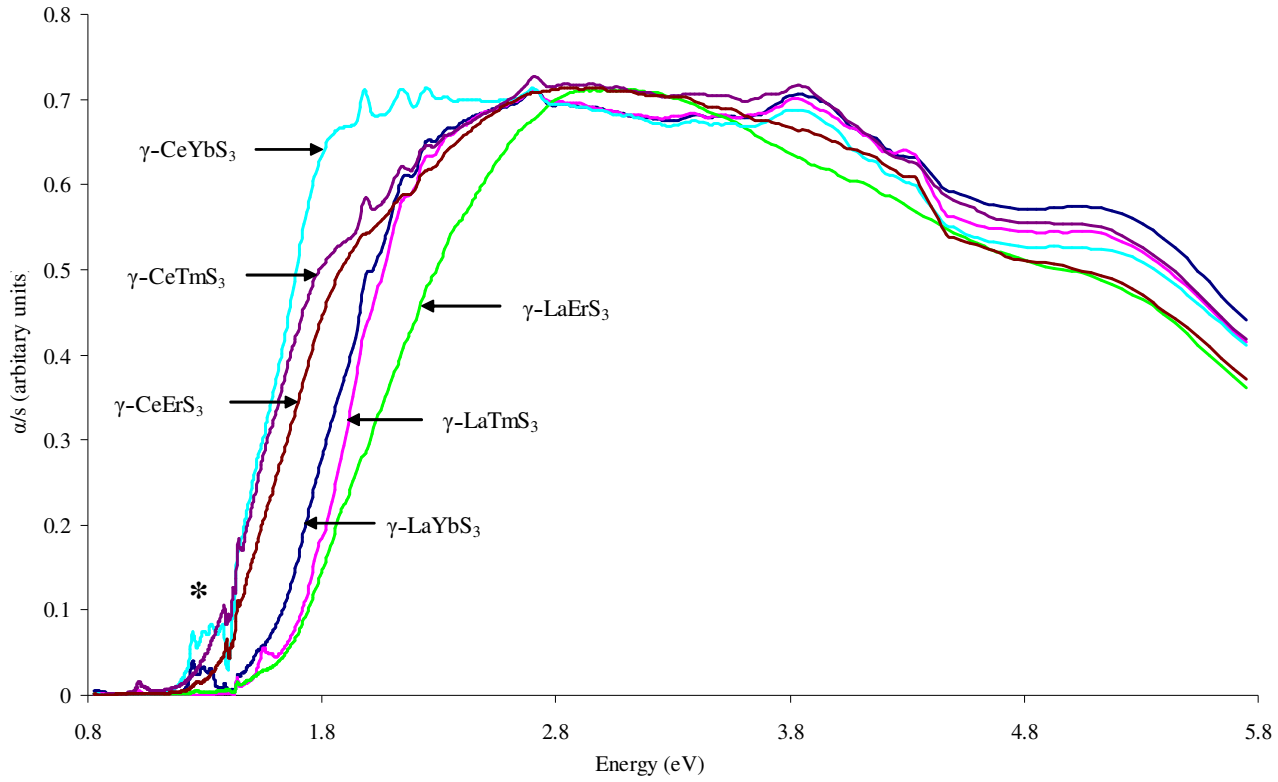
0.8
0.7
0.6
0.5
0.4
0.3
0.2
0.1
0
α/s (arbitary units)
γ-CeYbS3
γ-CeTmS3
γ-CeErS3
γ-LaErS3
γ-LaTmS3
γ-LaYbS3
*
0.8
1.8
2.8
3.8
4.8
5.8
Energy (eV)

Figure 6.

For Table of Contents Use Only

G. B. Jin, E. S. Choi, R. P. Guertin, J. S. Brooks, T. H. Bray, C. H. Booth, T. E. Albrecht-Schmitt

Chem. Mater. **2006**, *XX*, XXXX

Syntheses, Structure, Magnetism, and Optical Properties of the Ordered Mixed-Lanthanide Sulfides γ-$LnLn'S_3$ (Ln = La, Ce; Ln' = Er, Tm, Yb)

The layered mixed-lanthanide sulfides γ-$LnLn'S_3$ (Ln = La, Ce; Ln' = Er, Tm, Yb) have been prepared, and their structure and electronic properties have been measured. The magnetic susceptibility of these compounds may indicate geometric spin frustration. The band gaps for these materials can be changed as a function of the Ln^{3+} ion.

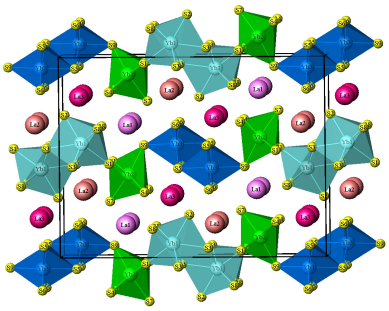

Table 1. Crystallographic Data for γ-LnLn'S_3 (Ln = La, Ce; Ln' = Er, Tm, Yb).

Formula	γ-$LaErS_3$	γ-$LaTmS_3$	γ-$LaYbS_3$	γ-$CeErS_3$	γ-$CeTmS_3$	γ-$CeYbS_3$
fw	402.35	404.02	408.13	403.56	405.23	409.34
Color	dark red	dark red	dark red	black	black	black
Crystal System	orthorhombic	orthorhombic	orthorhombic	orthorhombic	orthorhombic	orthorhombic
Space group	*Pnma* (No. 62)	*Pnma* (No. 62)	*Pnma* (No. 62)	*Pnma* (No. 62)	*Pnma* (No. 62)	*Pnma* (No. 62)
a (Å)	16.510(1)	16.4500(9)	16.410 (1)	16.4891(9)	16.459(1)	16.368(1)
b (Å)	3.9963(2)	3.9877(2)	3.9847 (3)	3.9705(2)	3.9704(3)	3.9562(2)
c (Å)	21.260(1)	21.215(1)	21.202 (2)	21.127(1)	21.091(2)	21.058(1)
V (Å^3)	1402.7(2)	1391.6(2)	1386.4 (3)	1383.1(2)	1378.3(3)	1363.6(2)
Z	12 (4)	12 (4)	12 (4)	12 (4)	12 (4)	12 (4)
T (K)	193	193	193	193	193	193
λ (Å)	0.71073	0.71073	0.71073	0.71073	0.71073	0.71073
ρ_{calcd} (g cm^{-3})	5.716	5.785	5.866	5.814	5.859	5.982
μ (cm^{-1})	279.71	292.28	303.80	289.74	301.21	315.00
R(F)[a]	0.0297	0.0282	0.0328	0.0270	0.0300	0.0286
$R_w(F_o^2)$ [b]	0.0692	0.0744	0.0672	0.0675	0.0735	0.0803

[a] $R(F) = \sum \| F_o | - | F_c \| / \sum | F_o |$ for $F_o^2 > 2\sigma(F_o^2)$. [b] $R_w\left(F_o^2\right) = \left[\sum \left[w\left(F_o^2 - F_c^2\right)^2 \right] / \sum w F_o^4 \right]^{1/2}$.